International Journal of Disaster Risk Reduction 108 (2024) 104561

Contents lists available at ScienceDirect

International Journal of Disaster Risk Reduction

journal homepage: www.elsevier.com/locate/ijdrr

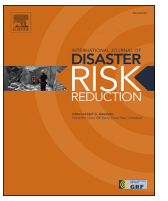

Prefecture-level health risk assessment for hot extremes in China

Junwang Huang [a, c], Shi Shen [a, b, c, *], Changxiu Cheng [a, b, c, d], Changqing Song [a, c]

[a] State Key Laboratory of Earth Surface Processes and Resource Ecology, Beijing Normal University, Beijing, 100875, China
[b] Key Laboratory of Environmental Change and Natural Disaster, Beijing Normal University, 100875, China
[c] Faculty of Geographical Science, Beijing Normal University, Beijing, 100875, China
[d] National Tibetan Plateau Data Center, 100101, China

ARTICLE INFO

Keywords:
Hot extremes
Health risk assessment
Risk zone
Prefecture level

ABSTRACT

Evaluating prefecture-level health risks for hot extremes is the core of localized adaptation measures to mitigate negative heat-related impacts. Here, by applying the heat hazard-human exposure-social vulnerability framework, we assessed the prefecture-level health risk for summertime hot extremes in China, with multisource data from 329 prefecture units. Regions suffering very high and high levels of health risk were observed in several main basins and plains, including the Turpan Basin, the North China Plain, the middle-lower Yangtze River Plain, the Pearl River Delta, the Chengdu Plain, and the Wei River Valley. Health risk structures were identified, and 72 prefecture units (22 %) were found in the risk zone of Hh-He-Hv (high heat hazard, high human exposure, and high social vulnerability), of which 44 % of sites were distributed in the North China Plain and must be prioritized for adaptation. The risk components of human exposure were the main drivers of health risk and its spatial heterogeneity. For the southeastern region, social vulnerability plays a more significant role than heat hazard. Four types of social vulnerability were summarized and will be useful for targeted adaptation plans. The assessment process will be insightful and can be applied in other countries or on a global scale.

1. Introduction

In the era of climate change, there is a relentless shattering of global warming records. The year 2023, surpassing 2016, has now become the warmest calendar year on record. According to the ERA5 dataset, 2023 exhibited a temperature 1.48 °C higher than the pre-industrial level of 1850–1900. Notably, each day throughout the year surpassed 1 °C above the pre-industrial level for that specific time of year, a historic first. Approximately 50 % of days exceeded 1.5 °C above the pre-industrial level, with two days in November registering over 2 °C warmer. This alarming acceleration of global warming also rendered the boreal summer (June–August) the warmest season ever recorded [1]. The surge in hot extremes emerged as a significant threat to worldwide human health, exacerbating vulnerabilities, particularly among those already displaced by complex conflicts [2–5]. The impacts are more pronounced at the local scale, especially in regions with high population exposure and vulnerable socioeconomic conditions [6,7]. Urgent measures, including local adaptation plans for hot extremes, are imperative to mitigate negative impacts and bolster local resilience [8,9].

The development and implementation of local risk reduction strategies for hot extremes have gained momentum since the adoption of the hazard-vulnerability-exposure framework proposed by the IPCC [10,11] for health risk assessment. Here, health risk is expressed as a function of the three components of hazard, exposure, and vulnerability, and the last component is the function of sensitivity and capacity. For hot extremes, the assessment of hazard focuses on accurately assessing the physical intensity of heat hazards,

* Corresponding author. State Key Laboratory of Earth Surface Processes and Resource Ecology, Beijing Normal University, Beijing, 100875, China.
E-mail address: shens@bnu.edu.cn (S. Shen).

https://doi.org/10.1016/j.ijdrr.2024.104561
Received 30 October 2023; Received in revised form 7 May 2024; Accepted 14 May 2024
Available online 17 May 2024

typically relying on air temperature data and indicators like high temperature days [12,13]. Some studies broaden the definition of heat hazards by incorporating additional indices such as land surface temperature (LST) and considering the health risks associated with nighttime hot extremes [14–16]. Regarding exposure, heat-related studies primarily focus on human exposure [17,18], using population density as a key indicators [19,20]. Vulnerability represents social vulnerability in heat-related reasearch [10,11], with varying indicators selected based on the "fit for purpose" principle in illuminating the features of interest in the complex coupled human-environment system [21]. For example, Zhang et al. [15] focused on elderly citizens in mountainous areas and took the conditions of vegetation and water bodies, terrain, housing, traffic, and medical facilities into consideration. Overall, both aspects of sensitivity and adaptability need to be considered in current assessments of social vulnerability. In detail, sensitivity focuses on people who are more susceptible to hot extremes; for instance, elderly or younger people have been considered more sensitive [22]. Adaptability refers to the ability of individuals or regions to cope with hot extremes, which is related to the natural and socioeconomic resources of a region [15].

The integration of the above heat hazard-human exposure-social vulnerability framework into health risk assessments for hot extremes over the past decade has showcased diversity in scale observations, indicator selections, and data integrations [19,23,24]. In China, community-level health risk assessments have been conducted in some typical megacities, such as Beijing [25], Wuhan [20], and Hong Kong [17,26]. Regional assessments have been carried out at the county-level in areas like Zhejiang Province [24], the Yangtze River Delta [12], and the Middle-Lower Yangtze River Plain [27]. Nationwide assessments encompassed county-level assessments in 2010 [28] and prefecture-level assessments in 2020 [13]. These researches further underscore the feasibility and multi-scale applicability of the framework. However, the dynamic nature of global spatial and temporal temperature patterns, coupled with varying socioeconomic conditions, necessitates a continuous reliance on up-to-date and relevant data. While existing studies often focus on regional scopes, some large-scale investigations fall short of adequately accounting for regional variations, highlighting a critical gap in understanding.

Moreover, many studies have directly calculated the hot extremes hazard and populations exposure at the prefecture scale, but there are spatial differences between hot extremes and population geographical distribution. On the one hand, there exists significant disparity in total population among prefecture-level units in China, between the eastern and western regions, as well as between large and small cities. On the other hand, within individual prefecture in China, there also exists considerable variation in population distribution, particularly in many medium-sized cities with large land areas in the western regions. In these areas, the bulk of the population tends to concentrate in the central urban areas, while the population density in the surrounding suburbs may be extremely low. It is necessary to consider hot extremes hazard and populations exposure considering population density.

In the contemporary landscape, risk management and the construction of resilient societies face significant scientific challenges, particularly in regions like China characterized by frequent hot extremes and vast territorial expanse [29]. The intricate interplay between topography and socioeconomic zones poses formidable challenges to effective risk management. Globally, spatial disparities in hot extremes and varying resilience among regions and groups raise concerns regarding global equity [30]. Low-income regions, contributing least to climate change, bear greater climate pressure and health risks, emphasizing the need for strategies that prioritize robust risk management and local adaptation planning [31]. Understanding the risk structure and identifying the dominant factors are crucial for effectively informing policy decisions and achieving desired policy outcomes [32,33].

To bridge the gap between risk assessment and local adaptation planning, some researchers have explored some practical applications [34]. For example, risk zoning in Wuhan has been highlighted as an essential tool for guiding urban planning and risk governance [20]. Dominant factor partitioning has guided targeted local adaptation planning [28], and models assessing the contribution of each component to health risks offer valuable insights [13]. However, these studies remain limited in scope, and further research is needed to address these gaps and enhance risk management practices.

Hence, this study introduces a comprehensive research conceptual flowchart for health risk assessment, encompassing the entire process of heat-related health risk assessment, including framework construction and mapping (method in Section 2.2, and analysis in Section 3.1), risk structure exploring (method in Section 2.3, and analysis in Section 3.2), and dominant factors identification (method in Section 2.4, and analysis in Section 3.3). First, drawing upon the heat hazard-human exposure-social vulnerability framework, this study constructed a comprehensive indicator system based on multiple data sources and assessed the health risk for hot extremes in 329 prefecture units across China during summer (June to August) of 2020. This article statistically analyzes and converges the hazards of hot extremes at the grid scale. Prefecture units were then classified into five levels based on their health risk values and the three components of heat hazard, human exposure, and social vulnerability. Next, we employed spatial autocorrelation model (i.e., Local Moran's I) to identify spatial patterns among prefecture units, and constructed risk zones to explore the risk structure across China. Ultimately, based on the Geographically weighted regression (GWR), we explore the dominant factors for hot extremes health risk and their spatial heterogeneities across China. This approach will contribute enhances the relevance of our findings for local adaptation planning.

2. Materials and methods

2.1. Study area and data

Located in east Asia, China is ranked 10th worldwide in terms of disaster risk in the World Risk Index 2023, a composite index that also includes risks from climate-related hazards (www.WorldRiskReport.org). Meanwhile, with its expansive territory, diverse topography and complex climate condition, China also shows great spatial heterogeneities in health risk for hot extremes. As shown in Fig. 1, China is categorized into 9 climate zones (Fig. 1a), and exhibits a distinctive three-tiered terrain, characterized by elevations ascending in the west and descending in the east (Fig. 1b). The distribution of major urban agglomerations is prominently concentrated

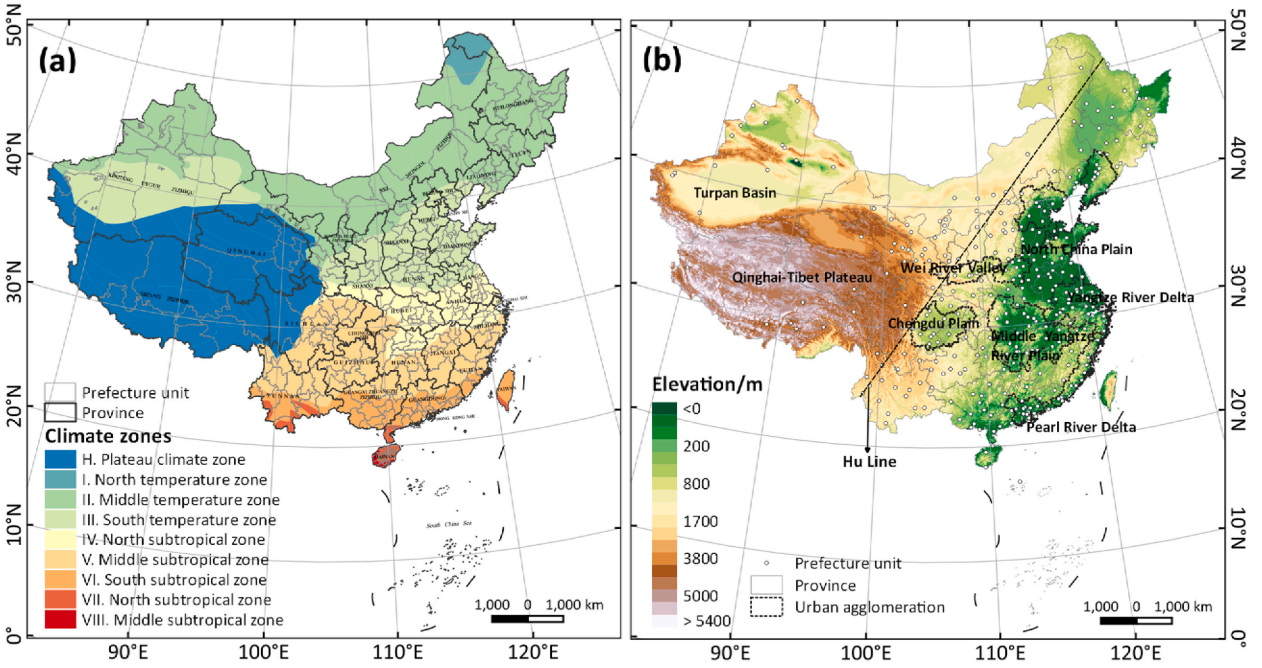

Fig. 1. Distribution of (a) prefecture units and climate zones, (b) three-tiered terrain, main topographic units and urban agglomerations in China.

in the plains and valleys, particularly in regions featuring relatively flat terrain. This urban development pattern is more prevalent in the eastern parts of the country and gradually diminishes towards the western regions.

Hourly temperature data covering June–August from 1991 to 2020 were obtained from the ERA5-Land reanalysis dataset by the European Centre for Medium-Range Weather Forecasts (ECMWF, https://cds.climate.copernicus.eu/). The dataset contains an hourly variable of the air temperature at 2 m above the ground (T_a, ˚C), and the spatial resolution is 0.1˚. Daily maximum temperature (TX) and minimum temperature (TN) could be extracted by hourly temperature data and counted for the number of high-temperature days and nights each year. Census total resident, youth, elderly, and illiterate population data at the city level for China (329 prefecture units in all) were obtained from China's Seventh (2020) National Census. Gridded population density data with a spatial resolution of 1 km in 2020 were obtained from the WorldPop dataset (https://hub.worldpop.org). Socioeconomic data for 2020 at the city level were obtained from China's National Bureau of Statistics (China City Statistical Yearbook 2021) and some local Bureaus of Statistics (e.g., Hangzhou Statistical Bulletin of National Economic and Social Development 2021). The Terra Moderate Resolution Imaging Spectroradiometer (MODIS) monthly enhanced vegetation index (EVI) data (MOD13A3) at a 1 km spatial resolution for the period of June–August 2020 were downloaded from the Earth Science Data Systems (ESDS) Program (https://www.earthdata.nasa.gov/).

2.2. Health risk framework construction

Based on the heat hazard-social vulnerability-human exposure framework, this study considered the indicators of the hot extremes' intensity, demographic characteristics and regional socio-economic conditions [19,20,24,35], to conduct health risk assessment (Table 1).

2.2.1. Heat hazard assessment

According to the China Meteorological Administration, a day with a maximum temperature higher than 35 ˚C is a high-temperature day, and a night with a minimum temperature higher than 26 ˚C is a high-temperature night. We used the temperature dataset over the past 30 years (1991–2020) to capture the long-term climate status, and the 90th percentile of high-temperature day/

Table 1
Components of health risk and their respective indicators used in this study.

Risk components		Indicators	Indicator nature
Heat hazard		Number of high-temperature days and nights (Hd)	+
Human exposure		Population density	+
Social vulnerability	Sensitivity	Proportion of children population (age <15 years)	+
		Proportion of elderly population (age ≥65 years)	+
		Proportion of illiterate population	+
	Capacity	Convenience to urban green space (enhanced vegetation index, EVI)	–
		Gross regional product (GDP) per capita	–
		Number of hospital beds per 10,000 people	–

night during the past 30 years was derived to represent the current intensity of daytime/nighttime hot extremes. Then the sum of high-temperature days and nights (Hd) during the summertime (June–August) were derived as the indicator of heat hazard. Specifically, the processing process includes the following four steps.

(1) The daily maximum temperature (TX) and daily minimum temperature (TN) of each day were extracted from hourly scale temperature data (ERA5_Land reanalysis data).
(2) The high-temperature days (TXd) and high-temperature nights (TNd) of each summer were extracted from the TX and TN datasets based on thresholds of 35 °C and 26 °C, respectively.
(3) Based on the probability distribution of TXd and TNd datasets during the past 30 years, the 90th percentile values were derived as TXd90 and TNd90. The sum of TXd90 and TNd90 was the final indicator (Hd) for heat hazard assessment.

2.2.2. Social vulnerability assessment

Social vulnerability to hot extremes is a critical aspect determined by two fundamental factors: sensitivity and capacity (see Table 1). The indicators for sensitivity included proportions of children, elderly individuals, and illiterate individuals, representing segments of the population particularly susceptible to the negative impacts of hot extremes. Capacity indicators were chosen to reflect the resources and capabilities that prefecture units equipped to cope with hot extremes, including the availability of urban green space, GDP per capita, and the number of hospital beds per ten thousand people. The enhanced vegetation index (EVI) was employed as the reliable indicator for the availability of urban green space. And the averaged EVIs for prefecture units were aggregated through zonal statistics.

2.2.3. Health risk assessment

Zonal statistics and normalization were the last two steps for prefecture-level risk components and health risk assessment. For zonal statistics, the border was the administrative boundary of each prefecture unit, and the statistic was the 90th value rather than the average.

Normalization is a crucial step in integrating multiple indicators for comparability and aggregation in health risk assessment. Traditional normalization methods scale data within the range of 0–1. However, assigning a value of 0 in this range represents the absence of risk, which may lead to inaccurate classifications of prefecture units with actual health risks for hot extremes. To address this issue, we improved the traditional Min-Max normalization method by distributing data within the range of 0.1–0.9 (Eq. (1)) [20]. For prefecture units without hot extremes or human presence, a value of 0 was maintained and excluded from the normalized list. For prefecture units with hot extremes and human presence, their values were normalized between 0.1 and 0.9, ensuring an accurate representation of risk distribution.

Population density was selected as the representative index for human exposure. The data processing process includes zonal statistics and normalization (Eq. (1)). Considering the lack of population density grid data in southern Tibet, especially in the prefecture units of Shannan and Nyingchi, the population density data came from China's Seventh (2020) National Census.

Additionally, we normalized the sensitivity indicators using Eq. (1), allowing for a higher sensitivity value to indicate a greater degree of social vulnerability. In contrast, the capacity indicators were normalized using Eq. (2), where higher values indicated a higher level of resilience and a lower level of social vulnerability. Finally, prefecture-level social vulnerability was derived by combining sensitivity and capacity indicators. This process entailed averaging the six selected indicators and applying normalization techniques. By refining the normalization approach, the assessment captured risk in prefecture units with hot extremes and represented the absence of risk in areas without hot extremes or human elements, yielding comprehensive and realistic results.

$$X' = 0.1 + \frac{X - MIN}{MAX - MIN} \times (0.9 - 0.1) \tag{1}$$

$$X' = 1 - \left[0.1 + \frac{X - MIN}{MAX - MIN} \times (0.9 - 0.1)\right] \tag{2}$$

Finally, the score of the health risk index for hot extremes was defined by the multiplication of the three equally weighted risk components:

$$HR = H \times E \times V \tag{3}$$

where HR is the integrated score of health risk, and H, E, and V are the normalized results of heat hazard, human exposure, and social vulnerability, respectively. Except for the value of 0, other HR values were finally normalized to 0.1 to 0.9. Data classification and appropriate sequential color schemes are effective in representing risk levels and spatial patterns across large regions [25]. In this study, the health risk values, excluding values of 0, were categorized into a five-level qualitative scale using an equal percentile grading method from high to low: very high (top 20 %), high (20%–40 %), moderate (40%–60 %), low (60%–80 %), and very low (last 20 %), along with the results of the three components of heat hazard, human exposure, and social vulnerability.

2.3. Health risk structure exploring

2.3.1. Local Moran's I

As one of the indicators of Local Indicators of Spatial Association (LISA) method [36], the Local Moran's I is a measure introduced by Anselin [37] that is widely used to identify spatial autocorrelation, i.e., the degree to which similar values of a variable are clus-

tered together in space. The Local Moran's I (univariate) is calculated for each observation in a dataset and represents the degree of clustering or dispersion of similar values around that observation, and it is given as follows:

$$I_i = \frac{x_i - X}{S_i^2} \sum_{j=1, j\neq i}^{n} w_{i,j}\left(x_j - X\right) \tag{4}$$

where x_i is an attribute for feature i,X is the mean of the corresponding attribute, $w_{i,j}$ is the spatial weight between feature i and j, and:

$$S_i^2 = \frac{\sum_{j=1, j\neq i}^{n} \left(x_j - X\right)^2}{n-1} \tag{5}$$

where n is equal to the total number of features. The Z_{I_i}-score for the statistics is computed as follows:

$$Z_{I_i} = \frac{I_i - \mathrm{E}\left[I_i\right]}{\sqrt{V\left[I_i\right]}} \tag{6}$$

where:

$$\begin{aligned} \mathrm{E}\left[I_i\right] &= -\frac{\sum_{j=1, j\neq i}^{n} w_{ij}}{n-1} \\ \mathrm{V}\left[I_i\right] &= \mathrm{E}\left[I_i^2\right] - \mathrm{E}\left[\boldsymbol{I}_i\right]^2 \end{aligned} \tag{7}$$

The bivariate Local Moran's I[38] was used to solve the multivariate spatial autocorrelation problem to disentangle whether the correlation between multiple variables at adjoining locations is due to the correlation among the variables, or a similarity due to being neighbors in space. In essence, it captures the relationship between the value for one variable at location i,x_i, and the average of the neighboring values for another variable, i.e., its spatial lag $\sum_j w_{ij}y_j$. Apart from a constant scaling factor (that can be ignored), the statistic is the product of x_i with the spatial lag of y_i (i.e., $\sum_j w_{ij}y_j$), with both variables standardized, such that their means are zero and variances equal one:

$$I_i^B = cx_i \sum_j w_{ij}y_j, \tag{8}$$

where w_{ij} are the elements of the spatial weights matrix. In GeoDa 1.20 software, we used 329 municipal units in the study area to construct a spatial weight matrix (Queen adjacency method). Based on this, univariate Local Moran's I analysis was performed for the three risk components of heat hazard, human exposure, and social vulnerability, respectively, and bivariate Local Moran's I analysis was performed for pairs of the three risk components.

2.3.2. Health risk zoning

Prefecture units were further classified into different risk zones based on the composition of the three components. To achieve this, all prefecture units were reclassified using standardized scores for each target layer. For example, for heat hazard risk, prefecture units in the top 50 % are classified as high risk of heat hazard, while the bottom 50 % are classified as low risk. The same approach has been applied to classify prefecture units based on human exposure and social vulnerability results.

Consequently, a total of eight risk zones were identified and named Hh-He-Hv, Hh-He-Lv, Hh-Le-Hv, Lh-He-Hv, Hh-Le-Lv, Lh-He-Lv, Lh-Le-Hv, and Lh-Le-Lv. In these names, the left side (H and L) indicates the assessment level, with high and low representing higher and lower risk levels, respectively. The right side (h, e, and v) represents the assessment layers: heat hazard, human exposure, and social vulnerability, respectively. This classification of risk zones provides a comprehensive understanding of the spatial variations in the risk composition, enabling policymakers and stakeholders to prioritize interventions and resources based on the specific risk profiles of different areas.

2.4. Geographically weighted regression (GWR)

Geographically weighted regression (GWR) [38] provides spatially varying coefficient estimates via location-specific weighted regression model calibrations, to explore spatial heterogeneities or nonstationarities, quantitatively. Here, we tried to use it to explore the dominant factors for hot extremes health risk and their spatial heterogeneities across China. The GWR model is expressed as follows:

$$Y_i = \beta_{i0} + \Sigma_k \beta_{ik} X_{ik} + \varepsilon_i, i = 1, 2, \cdots, n. \tag{9}$$

Here, β_i represents the regression coefficients of the response of the sample point with respect to the k-th independent variable, ε is the random error term, k is the subscript for the independent variable parameter, and n is the number of samples to be calculated. If

the regression coefficients do not vary with changes in sample points, then geographically weighted regression is equivalent to linear regression. The regression coefficients of the geographically weighted regression model can be calculated using the least squares method by introducing the weight matrix W_i, and is expressed as follows:

$$\beta_i = \left[\boldsymbol{X}^{\mathrm{T}}\boldsymbol{W}_i\boldsymbol{X}\right]^{-1}\boldsymbol{X}^{\mathrm{T}}\boldsymbol{W}_i\boldsymbol{Y}. \tag{10}$$

Here, β_i is the estimated regression coefficient for sample point i, X is the observed matrix of independent variables, Y is the observed vector of dependent variables, and W_i is a spatial weight diagonal matrix composed of weight W_{ij}. W_i is represented as follows:

$$\boldsymbol{W}_i = \begin{pmatrix} w_{i1} & 0 & \cdots & 0 \\ 0 & w_{i2} & \cdots & 0 \\ \vdots & \vdots & & \vdots \\ 0 & 0 & \cdots & w_{in} \end{pmatrix} \tag{11}$$

Here, $w_{ij}j = 1,2,\ldots,n$ represents the weight values of sample point j relative to sample point i. Taking the health risk values as the dependent variable, and their risk components of heat hazard, human exposure, and social vulnerability as the explanatory variables, the GWR model (Gauss function for spatial weight, fixed bandwidth with AICs method) was run in ArcGIS 10.8 software for the prefecture units with hot extremes.

3. Results

3.1. Distribution of health risk and risk components for hot extremes

As shown in Fig. 2a, the basins, southern plains, and deltas emerged as the regions in China most severely affected by hot extremes, exhibiting the highest level of heat hazard. Regions with very high levels of heat hazard located in Xinjiang Province, as well as the middle-lower Yangtze Plain, the Pearl River Delta, the Wei River Valley, and certain areas in southern Guangxi and Hainan, where exhibited the highest number of high-temperature days and nights (Hd) in China (Fig. S1c). Notably, Xinjiang Province experienced the highest number of hot extremes in the daytime across China (Fig. S1a), while the southern regions encountered more nighttime hot extremes (Fig. S1b). The North China Plain and the Chengdu Plain also suffered more hot extremes than the surroundings and were categorized as high level of heat hazard.

The analysis of human exposure risk in China revealed a distinct and geographically patterned distribution, following a northwest-southeast gradient that aligned broadly with the Hu Line (Fig. 2b). Prefecture units characterized by a very high level of human exposure were predominantly concentrated in the major urban agglomerations, including the North China Plain, southeastern coastal areas, and in several provincial capitals in midwest regions, such as Chengdu and Nanchang.

Prefecture units exhibiting a very high level of social vulnerability were mainly dispersed in western China, the North China Plain, and Guangxi Province (Fig. 3c). In contrast, prefecture units in northeastern China and the eastern coast generally demonstrated lower levels of social vulnerability. Moreover, several provincial capitals, such as Chengdu, Nanning, and Jinan, as well as relatively developed prefecture units within provinces, exhibited noticeably lower levels of social vulnerability than their surroundings. In northeastern China, it's noteworthy that very few units were classified as having high or very high levels of social vulnerability. This unique pattern can largely be attributed to several factors: a lower proportion of children (see Fig. S3a) and illiterate individuals (see Fig. S3b), as well as improved availability of urban green spaces (see Fig. S3d) and hospital services (see Fig. S3f). Similarly, besides the eastern coastal regions, the low and very low levels of social vulnerability are primarily due to a reduced proportion of children (see Fig. S3a) and higher GDP per capita (see Fig. S3e).

Fig. 3d illustrates the spatial distribution of health risk for hot extremes, revealing higher health risks in eastern and southern China, as well as in Xinjiang Province, where major basins and plains are located, including the Turpan Basin, the North China Plain, the middle-lower Yangtze River Plain, the Pearl River Delta, the Chengdu Plain, and the Wei River Valley. Specifically, as shown in Table S1, we found that Guangdong accounting for 7 out of the top 10 cities, while the remaining 3 cities were situated in the Yangtze River Delta, and Shanghai emerged as the city with the highest health risk within there.

3.2. Analysis of the risk structure

3.2.1. The spatial autocorrelation among risk components

As shown in Fig. 3a, b, and c, the calculation results of the univariate Local Moran's I indicate significant positive spatial autocorrelation within each of the three risk components. Notably, the spatial autocorrelation of heat hazard (Fig. 3a) is most pronounced, with an overall Moran's index of 0.81. It forms large high-high clusters in 58 prefecture units in the of the Middle-lower Yangtze River Plain, and smaller high-high clusters are distributed in Xinjiang and the Pearl River Delta. This suggests the great spatial correlation in the high level of heat hazard in these three regions. Low-low clusters (86 prefecture units) are concentrated in the southwest and northeast of China, most of which experienced few high-temperature days or nights. The assessment of human exposure (Fig. 3b) reveals large low-low clusters in the north of the Hu Line, comprising 84 prefecture units, while high-high clusters concentrate in the Yangtze River Delta and Pearl River Delta, renowned for their high population density. It is noteworthy that the cluster map does not detect high-high clusters in the North China Plain, where also have more human exposure than surroundings as shown in Fig. 2b. The assessment of social vulnerability (Fig. 3c) shows that high-high clusters are concentrated in the western China and at the four-

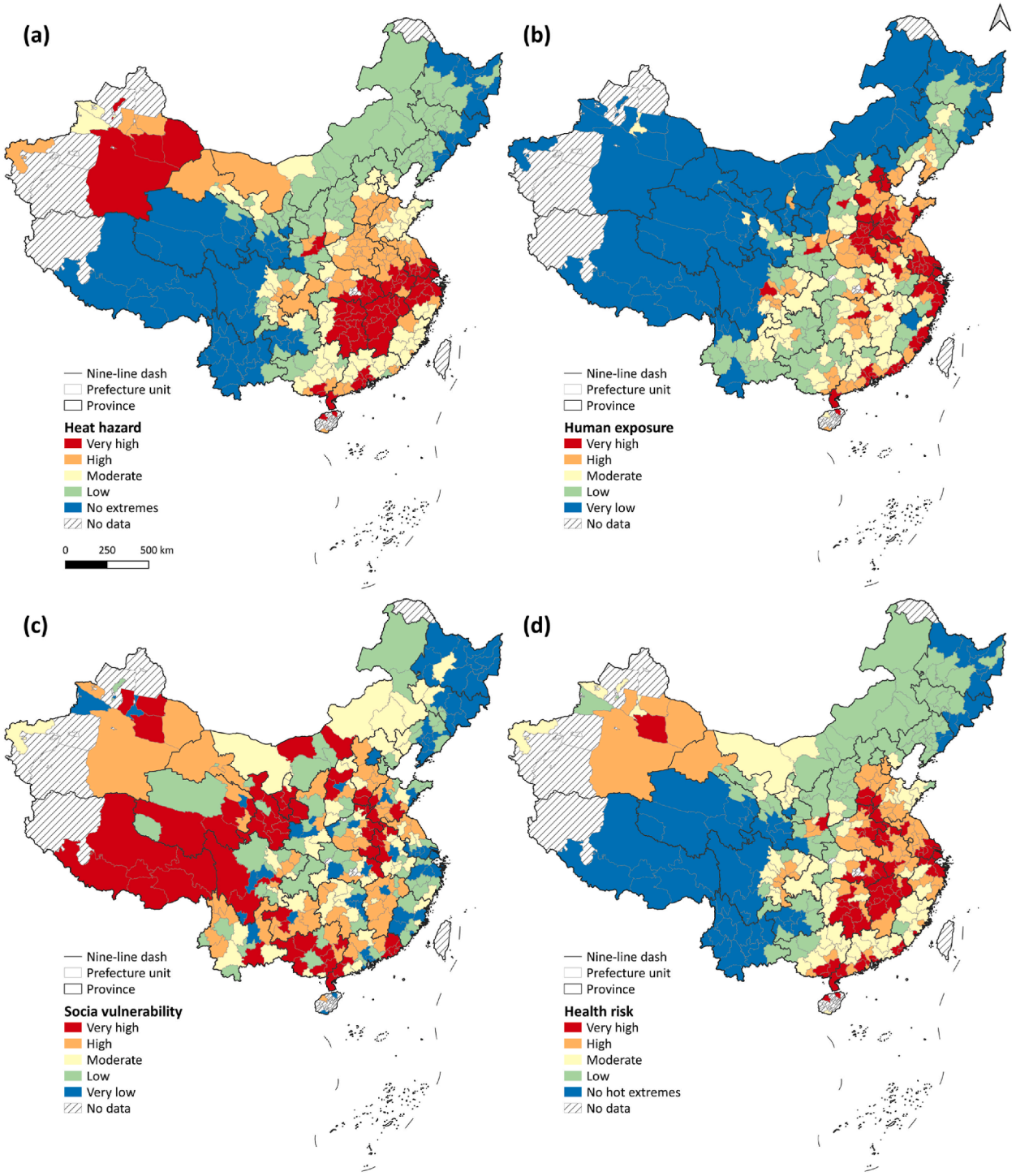

Fig. 2. Distribution of the health risk components of (a) heat hazard, (b) human exposure, (c) social vulnerability, and (d) health risk for hot extremes in China.

province boundary in the North China Plain, indicating the spatial correlation in high social vulnerability. In contrast, low-low clusters are concentrated in the northeastern China and Yangtze River Delta. All three components exhibit numerous significant high-high and low-low clusters, with few outliers, indicating distinct regional characteristics where clusters often share similar topographical, climatic, and socio-economic features.

The results of bivariate Local Moran's I for pairs of the three risk components are shown in Fig. 3d, e, and f. Heat hazard and human exposure exhibit a certain positive spatial autocorrelation, with an overall Moran's I of 0.26 (Fig. 3d). Low-low clusters of 77 pre-

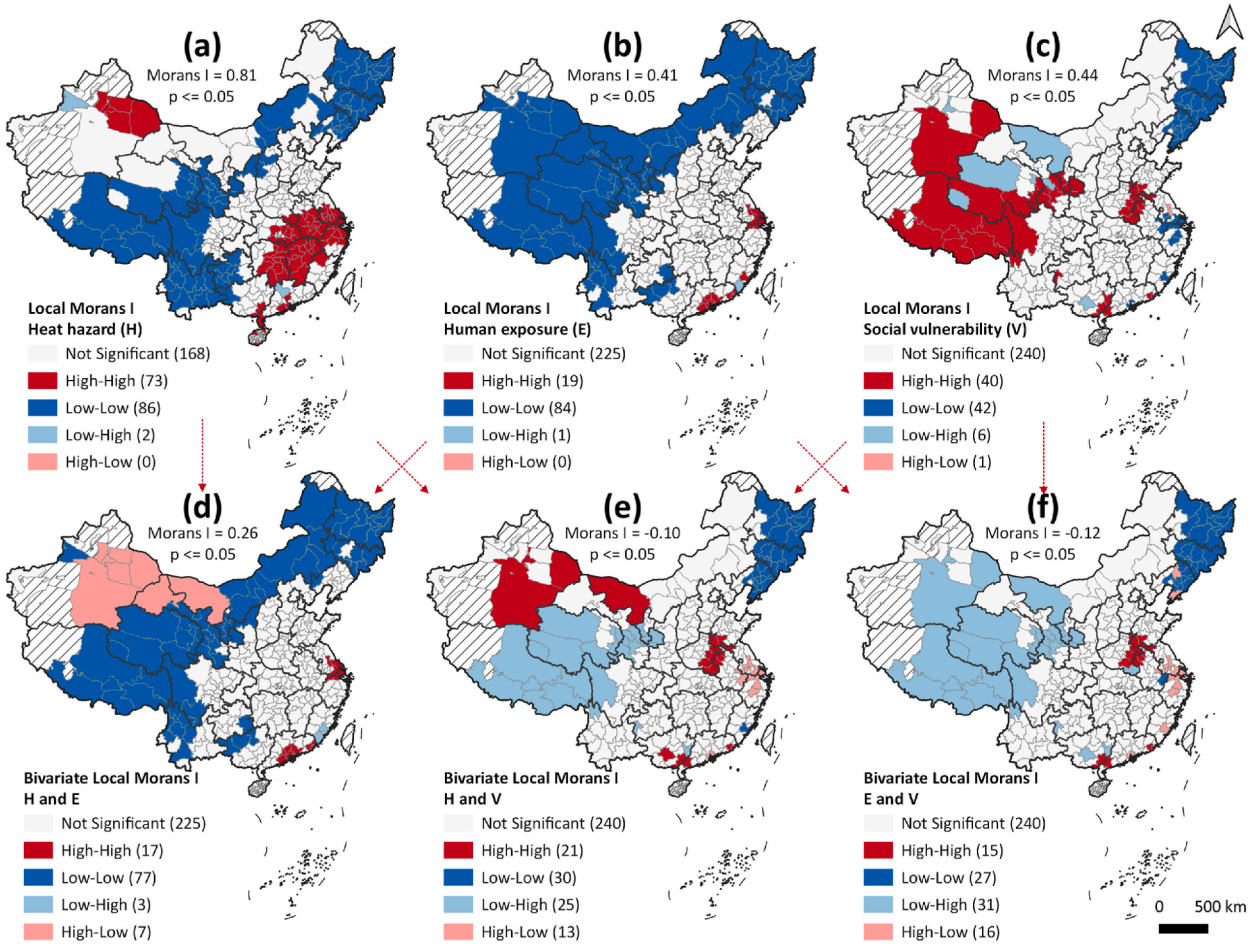

Fig. 3. Cluster map of univariate Local Morans I analysis for (a) heat hazard (H), (b) human exposure (E), (c) social vulnerability (V), and bivariate Local Morans I analysis for (d) H and E, (e) H and V, (f) E and V. The cluster map show in $p \leq 0.05$.

fecture units are concentrated in the southwest to northeast of China, indicating spatially similarly lower level of both heat hazard and human exposure in these areas. Xinjiang shows concentrated high-low outliers, reflecting higher level of heat hazard but lower level of human exposure. Few high-high clusters (17 prefecture units) are concentrated in the Yangtze River Delta and Pearl River Delta, indicating spatially correlated higher level of both heat hazard and human exposure. The overall Moran's I for heat hazard and social vulnerability is −0.10, attributed to numerous outliers in the southwest and Yangtze River Delta regions (Fig. 3e). The southwestern China exhibits low-high outliers, indicating spatially similar lower level of heat hazard but higher level of social vulnerability. Conversely, the high-low outliers in the Yangtze River Delta suggest a spatially correlated phenomenon of higher heat hazard but lower social vulnerability. The overall Moran's I for human exposure and social vulnerability is also negative, with large low-high outliers in the southwestern China, indicating clear spatial similarity in lower level of human exposure but higher level of social vulnerability (Fig. 3f). High-high clusters are concentrated in the four-province boundary in North China Plain, where the univariate Local Moran's I analysis did not detect high-high clusters for human exposure, suggesting spatially correlated higher level of human exposure and social vulnerability, as its overall level of heat hazard is not low, ultimately placing its health risk at the highest national level. Low-low clusters are concentrated in the northeast of China, indicative of a typical low-risk area with low heat hazard, low human exposure, and low social vulnerability (3L-type risk). High-low outliers are mainly distributed in the Yangtze River Delta, combining the previous two maps, the Yangtze River Delta is a typical area with high heat hazard, high human exposure, and low social vulnerability. The exceptionally lower social vulnerability in some areas (such as Hangzhou) is a major reason for the final health risk level being significantly lower than the levels of the first two risk components.

3.2.2. Risk zones for hot extremes health risk

As shown in Fig. 4, we classified 329 prefecture units into eight health risk zones and counted the number of prefecture units in different risk zones. Accounting for 79 % of prefecture units were in the risk zones of Hh-He-Hv (3H-type), Hh-He-Lv, Lh-Le-Hv, and Lh-Le-Lv (3L-type), with counts of 72, 59, 65, and 65, respectively. Focusing on these four zones, most prefecture units in the Hh-He-Hv and Hh-He-Lv risk zones were in eastern and southern China and in Xinjiang Province.

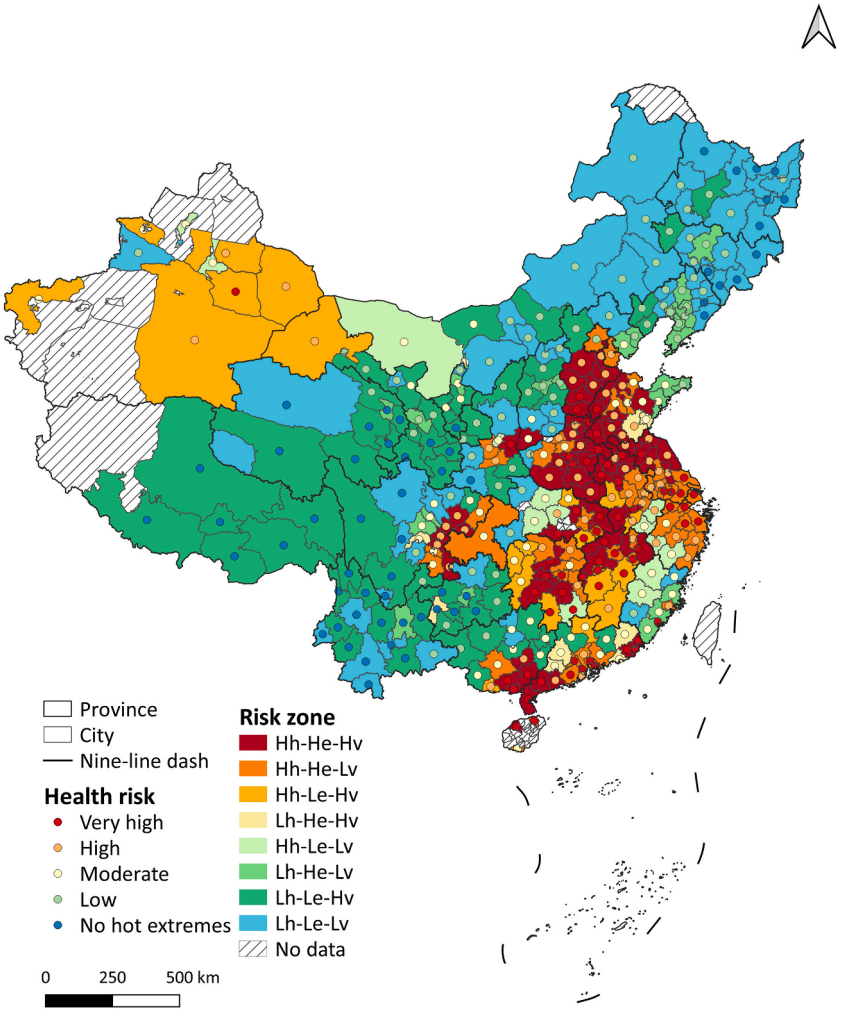

Fig. 4. Distribution of health risk and risk zones. The results of each prefecture units were shown in Table S1.

Prefecture units in the Hh-He-Lv risk zone had advantageous geographical locations (e.g., urban aggregations, provincial capitals), high GDP per capita, and a low proportion of vulnerable populations (see Fig. S3). However, due to widespread commercial and residential land, these prefecture units had strong heat hazards and high human exposure.

In contrast, prefecture units in the Hh-He-Hv risk zone were mainly located in the North China Plain (32 out of 72, 44 %), the middle Yangtze River Plain and southern Guangxi, where they experience high heat hazards and human exposure, while socioeconomic resources are inadequate, and the proportion of the child population is high, resulting in high social vulnerability.

Prefecture units in the Lh-Le-Hv and Lh-Le-Lv risk zones were mainly located in southwestern and northeastern China, and most Lh-Le-Lv risk zones were in the northeast, with a lower proportion of children and an illiterate population, as well as better availability of urban green spaces and hospital services.

3.3. Analysis of the determinations of risk components and their spatial heterogeneities

In the GWR model conducted for the 273 prefecture units with hot extremes, the coefficients of the explanatory variables to some extent indicate the degree to which each variable determines the final simulation results. Table 2 presents the statistical values of the coefficients for the three explanatory variables, and their spatial distribution is depicted in Fig. 5. The coefficient values for heat haz-

Table 2
The GWR coefficient of explanatory variables.

Explanatory variable	Average	Standard deviation	Max	Min
Heat hazard	0.50	0.04	0.41	0.60
Human exposure	0.99	0.23	1.35	0.32
Social vulnerability	0.53	0.19	0.77	0.17

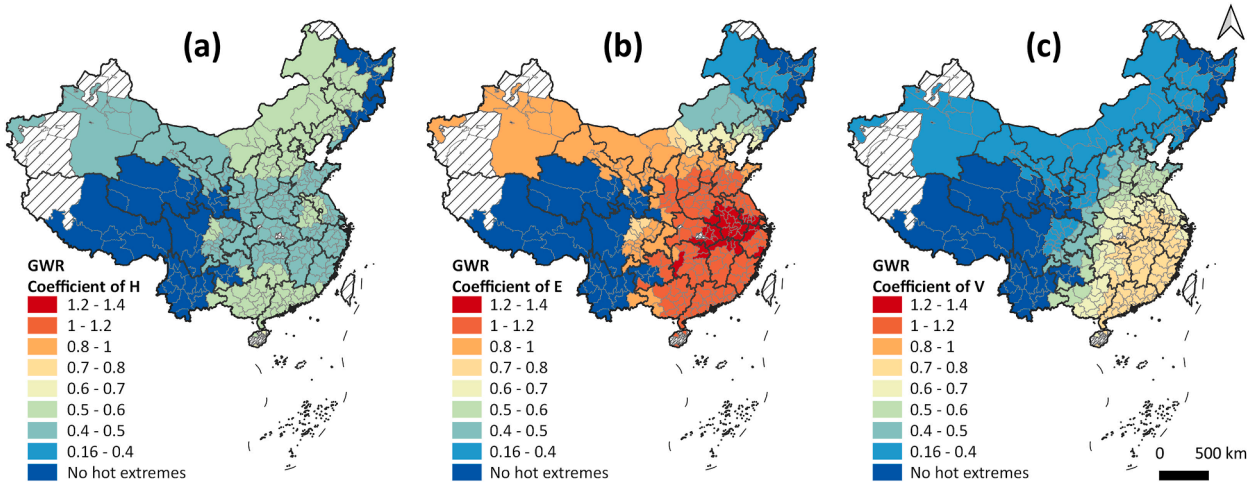

Fig. 5. Distribution of the GWR coefficient of explanatory variables of (a) heat hazard, (b) human exposure, and (c) social vulnerability in China (for the 273 prefecture units with hot extremes).

ard exhibit a relatively narrow range, between 0.41 and 0.60, with an average of 0.5. The spatial differences nationwide are not substantial (Fig. 5a). The coefficients in the eastern and central regions, as well as in Xinjiang, are slightly lower, ranging from 0.4 to 0.5, while the remaining areas fall within the range of 0.5–0.6.

In contrast, the coefficient range for human exposure exceeds 1.0, spanning from 0.32 to 1.35, with the highest average among the three variables at 0.99. This indicates that human exposure, overall, has the most significant impact on the assessment results of health risks. The spatial distribution map (Fig. 5b) reveals that coefficients in the eastern and southern regions often surpass 1.0, particularly in the Middle Yangtze River (Anhui Province and surrounding areas), even exceeding 1.2. The northwestern region follows, with values ranging between 0.8 and 1.0, while coefficients decrease towards the north in the northeast region, ranging from 0.8 to 0.3. This suggests that for regions out of northeastern China, human exposure is the most influential component for health risks, especially in the generally high-population density areas of eastern and southern China.

The values for social vulnerability range from 0.77 to 0.17, with an average of 0.53, slightly higher than heat hazard. The spatial distribution exhibits a clear decreasing trend from southeast to northwest (Fig. 5c). The five southeastern provinces (Zhejiang, Anhui, Jiangxi, Fujian, Guangdong) have the highest values, exceeding 0.7, while the northwestern and northeastern regions decrease to below 0.4. This implies that for the southeastern region, social vulnerability plays a more significant role in determining health risk than heat hazard. In contrast, for the northwestern and northeastern regions, the influence of heat hazard is slightly higher than that of social vulnerability.

4. Discussion

4.1. Comparison of assessment results with previous studies

The heat hazard-human exposure-social vulnerability framework, established and widely accepted in past studies, serves as the foundation for heat-related health risk assessment. However, variations in indicator selection yield different assessment results in the three risk components. Compared with previous nationwide assessments in China [13,28], our study revealed higher heat hazard risks in southern Guangdong and Guangxi and lower heat hazard risks in the mountain areas in southeastern China (see Fig. 2), and these results were attributed to the inclusion of nighttime hot extremes (see Fig. S1b). Further variations in indicator selection led to greater differences in spatial patterns of social vulnerability. Our findings closely corresponded to Xie et al.'s study [13], detecting higher vulnerability risks in the western China, and the North China Plain.

Similar gradients in health risks were observed with past studies [13,28], with the highest risks in eastern and southern China and in Xinjiang Province. However, health risks in the North China Plain and the southern regions of Guangdong and Guangxi may be underestimated due to the underestimation of heat hazard and social vulnerability risks. Additionally, barely significant differences in past studies were identified in the north of the Hu Line, except for Xinjiang Province. The choice of grading and mapping methods may be the main reasons that affect the results and lead to visual discrepancies.

In summary, our study's distribution of health risks aligns with previous studies, validating the consistency of findings. However, there is evidence to suggest that health risks may be underestimated in the North China Plain and southern Guangdong and Guangxi Provinces in past studies. Moreover, our study reveals greater spatial heterogeneity and regional differentiation, providing more accurate detection of hotspots, which adds value to its utilization.

4.2. Understanding of risk structure and dominate risk component for health risk

As the essential link between risk assessment and risk governance, risk structure and dominate components identification can be practical and efficient in formulating and implementing local adaptation plans at the prefecture level. Based on the spatial autocorre-

lation and risk zoning maps, we could pinpoint areas with high health risks and risk components. Prefecture units within the same risk zone exhibited similar risk structures and, in some regions, clustered together, suggesting the potential for adopting similar regional adaptation plans. The similarity between risk zones also provides reference and learning opportunities for improving specific factors.

With 79 % of prefecture units falling within the risk zones of Hh-He-Hv (3H-type), Hh-He-Lv, Lh-Le-Hv, and Lh-Le-Lv (3L-type), it becomes apparent that regardless of social vulnerability levels, the heat hazard and human exposure levels in most prefecture units often align. Despite differing grading criteria, spatial distribution maps linking these factors reveal more intersections of high levels in eastern China and increased low-level overlap from the northeast to the southwest regions. The spatial correlations of the bivariate Local Moran's I based on numerical results further confirm higher spatial autocorrelation and more clusters of heat hazard and human exposure. For the reason, maybe influenced by China's climatic foundation and urban distribution shaped by terrain and latitude, regions such as eastern, southern, and Xinjiang are more susceptible to extreme high temperatures, particularly in plain and valley areas, while these areas also suitable for urban development and resulting higher population exposure.

In contrast, when comparing the relationships of social vulnerability with heat hazard and human exposure, risk zoning results indicate a close probability of risk levels being consistent or opposite, and the analysis results of the bivariate Local Moran's I also show more outliers. The main reason is the imbalance in the development and allocation of social resources in China, including the imbalance between the eastern and western regions and the imbalance between provincial capital units and other units. We can categorize four typical regions based on social vulnerability: the Qinghai-Tibet Plateau with high vulnerability due to slow economies and a high proportion of vulnerable populations, the North China Plain with high vulnerability due to dense populations and inadequate social resources, northeastern China with low vulnerability due to low population density and relatively sufficient social resources, and the southeast coastal regions of Zhejiang and Fujian with low vulnerability characterized by dense populations, while strong economies, and a low proportion of vulnerable populations. Tailoring adaptation plans to these vulnerability types and focusing on capacity improvement and sensitivity reduction can enhance effectiveness in risk reduction and resilience building.

In our study, we discovered that among prefecture units with high or very high levels of health risk (top 40 %), nearly all of them were situated in the Hh-He-Hv and Hh-He-Lv zones (114 out of 132, 86 %), and the analysis results of GWR suggest that human exposure may be the determining factor. Consequently, reducing human exposure to a greater extent to alleviate the population pressure in areas with excessively high population density emerges as the most effective measure to mitigate health risks. Furthermore, for the southeastern regions, the determining factor of social vulnerability will also surpass hazard, and this trend intensifies towards the south. This phenomenon arises from the fact that in these regions, heat hazard levels are generally high, and the disparities in results are predominantly influenced by social vulnerability. Social vulnerability, in turn, exhibits greater spatial heterogeneity, thus indicating a stronger determinacy. Consequently, strategic enhancement of adaptability and reduction of sensitivity, coupled with risk zoning and regional development efforts, can significantly enhance the management of heat-related health risks.

4.3. Limitations and future directions

The assessment results are subject to the influence of the grading method, indicator selection, and weighting, as discussed previously. Given the extensive number of prefecture units in China, the variations in data distribution among indices, and the need for appropriate color schemes, this study employed equal-interval classification to depict the evaluation results. Although this approach may not fully capture the continuous gradient of the data, it effectively portrayed the overall spatial pattern of health risks across China. Meanwhile, the incorporation of auxiliary LISA analysis enabled the identification of hot spots, ensuring comprehensive coverage of high health risk clusters. Consequently, the assessment results exhibit a satisfactory level of accuracy and reliability, thereby offering valuable insights and guidance for risk assessment and management endeavors.

Moreover, in the face of global warming, the rising occurrence of hot extremes poses an increased heat hazard risk, especially in the nighttime. Therefore, nighttime hot extremes should be given greater consideration in risk assessments of heat hazards. And regions characterized by low risk of heat hazard while high risk of social vulnerability, such as Qinghai-Tibet Plateau, are likely to experience amplified health risks if hot extremes become more prevalent in the future.

5. Conclusion

Within the framework of identifying the key components of health risk—namely heat hazard, human exposure, and social vulnerability—this study amalgamated updated multisource data and constructed a comprehensive indicator system to evaluate health risks during summertime (June to August) in 329 cities across China. Utilizing risk structure and dominant component identification proved to be effective methods in bridging the gap between risk assessment and risk governance.

Regions experiencing very high and high levels of health risk were observed in several primary plains, including the Turpan Basin, the North China Plain, the middle-lower Yangtze River Plain, the Pearl River Delta, the Chengdu Plain, and the Wei River Valley. A noteworthy finding was that 79 % of prefecture units fell within the risk zones of Hh-He-Hv (3H-type), Hh-He-Lv, Lh-Le-Hv, and Lh-Le-Lv (3L-type), with counts of 72, 59, 65, and 65, respectively. Of these, 44 % of 3H-type units were concentrated in the North China Plain, making it imperative to prioritize adaptation efforts in this region. Human exposure emerged as the primary driver of health risk and exhibited significant spatial heterogeneity. Notably, in the southeastern region, social vulnerability played a more substantial role than heat hazard. The study identified four types of social vulnerability, offering valuable insights for targeted adaptation plans. This assessment process holds promise for application in other countries or on a global scale.

Future research on health risk assessments for hot extremes should prioritize developing countries such as China. With the ongoing effects of global warming, it is expected that more developing nations will confront increasingly severe hot extremes. However, their economies, marked by high social vulnerability, may not progress rapidly enough to mitigate the rising health risks linked to hot

extremes, thus exacerbating global inequality. Therefore, efficient and accurate assessment of hot extreme health risks, along with the detection of risk structures and determining factors, is needed. These assessments can assist decision-making bodies in formulating more effective local adaptation plans.

CRediT authorship contribution statement

Junwang Huang: Writing – review & editing, Writing – original draft, Software, Methodology, Investigation, Data curation. **Shi Shen:** Writing – review & editing, Supervision, Resources. **Changxiu Cheng:** Supervision, Project administration, Funding acquisition. **Changqing Song:** Supervision, Resources, Project administration, Funding acquisition.

Declaration of competing interest

The authors declare the following financial interests/personal relationships which may be considered as potential competing interests: Shi Shen reports financial support was provided by Beijing Normal University.

Data availability

Data will be made available on request.

Acknowledgments

Supported by the National Key Research and Development Program of China [No. 2019YFA0606901], the National Natural Science Foundation of China [No.42230106 and No.42201498], the Strategic Priority Research Program of the Chinese Academy of Sciences [No. XDA23100303].

Appendix A. Supplementary data

Supplementary data to this article can be found online at https://doi.org/10.1016/j.ijdrr.2024.104561.

References

[1] The Copernicus Climate Change Service (C3S). Global Temperatures: 2023 Warmest Year on Record, Close to 1.5°C above Pre-Industrial Level. https://climate.copernicus.eu/global-climate-highlights-2023..
[2] S. Perkins, L. Alexander, J. Nairn, Increasing frequency, intensity and duration of observed global heatwaves and warm spells, Geophys. Res. Lett. 39 (2012).
[3] S. Campbell, T.A. Remenyi, C.J. White, F.H. Johnston, Heatwave and health impact research: a global review, Health Place 53 (2018) 210–218.
[4] J.H. Stillman, Heat waves, the new normal: summertime temperature extremes will impact animals, ecosystems, and human communities, Physiology 34 (2019) 86–100.
[5] E.P. Petkova, H. Morita, P.L. Kinney, Health impacts of heat in a changing climate: how can emerging science inform urban adaptation planning? Current epidemiology reports 1 (2014) 67–74.
[6] C. Mora, et al., Global risk of deadly heat, Nat. Clim. Change 7 (2017) 501–506.
[7] D. Wang, et al., The impact of extremely hot weather events on all-cause mortality in a highly urbanized and densely populated subtropical city: a 10-year time-series study (2006–2015), Sci. Total Environ. 690 (2019) 923–931.
[8] Z. Zommers, K. Alverson, Resilience: the Science of Adaptation to Climate Change, Elsevier, 2018.
[9] L. Georgeson, M. Maslin, M. Poessinouw, S. Howard, Adaptation responses to climate change differ between global megacities, Nat. Clim. Change 6 (2016) 584–588.
[10] Climate change 2014, Impacts, Adaptation, and Vulnerability: Working Group II Contribution to the Fifth Assessment Report of the Intergovernmental Panel on Climate Change, Cambridge University Press, 2014.
[11] H.-O. Pörtner, et al., Climate Change 2022: Impacts, Adaptation and Vulnerability, IPCC, Geneva, Switzerland, 2022.
[12] Q. Chen, M. Ding, X. Yang, K. Hu, J. Qi, Spatially explicit assessment of heat health risk by using multi-sensor remote sensing images and socioeconomic data in Yangtze River Delta, China, Int. J. Health Geogr. 17 (2018) 1–15.
[13] X. Wen, P. Zhang, E. Dai, High temperature risk assessment at the municipal scale in China, Journal of Resources and Ecology 14 (2023).
[14] S. Russo, J. Sillmann, A. Sterl, Humid heat waves at different warming levels, Sci. Rep. 7 (2017) 7477.
[15] W. Zhang, C. Zheng, F. Chen, Mapping heat-related health risks of elderly citizens in mountainous area: a case study of Chongqing, China, Sci. Total Environ. 663 (2019) 852–866.
[16] G. Jendritzky, R. de Dear, G. Havenith, UTCI—why another thermal index? Int. J. Biometeorol. 56 (2012) 421–428.
[17] J. Song, B. Huang, J.S. Kim, J. Wen, R. Li, Fine-scale mapping of an evidence-based heat health risk index for high-density cities: Hong Kong as a case study, Sci. Total Environ. 718 (2020) 137226.
[18] M. Morabito, et al., Urban-hazard risk analysis: mapping of heat-related risks in the elderly in major Italian cities, PLoS One 10 (2015) e0127277.
[19] R.C. Estoque, et al., Heat health risk assessment in Philippine cities using remotely sensed data and social-ecological indicators, Nat. Commun. 11 (2020) 1581.
[20] J. Dong, et al., Heatwave-induced human health risk assessment in megacities based on heat stress-social vulnerability-human exposure framework, Landsc. Urban Plann. 203 (2020) 103907.
[21] A. de Sherbinin, et al., Climate vulnerability mapping: a systematic review and future prospects, WIREs Climate Change 10 (2019).
[22] Q. Zhu, et al., The spatial distribution of health vulnerability to heat waves in Guangdong Province, China, Glob. Health Action 7 (2014) 25051.
[23] C. Buscail, E. Upegui, J.-F. Viel, Mapping heatwave health risk at the community level for public health action, Int. J. Health Geogr. 11 (2012) 1–9.
[24] K. Hu, X. Yang, J. Zhong, F. Fei, J. Qi, Spatially explicit mapping of heat health risk utilizing environmental and socioeconomic data, Environ. Sci. Technol. 51 (2017) 1498–1507.
[25] X. Su, F. Wang, D. Zhou, H. Zhang, Heat health risk and adaptability assessments at the subdistrict scale in metropolitan beijing, Int J Disaster Risk Sci (2022), https://doi.org/10.1007/s13753-022-00449-8.
[26] J. Hua, X. Zhang, C. Ren, Y. Shi, T.-C. Lee, Spatiotemporal assessment of extreme heat risk for high-density cities: a case study of Hong Kong from 2006 to 2016, Sustain. Cities Soc. 64 (2021) 102507.
[27] H. Fu, F. Deng, H. Yang, N. Xu, J. Zhang, Assessing heat wave risk of urban agglomeration in the middle - lower Yangtze River based on remote sensing, Resour. Environ. Yangtze Basin (2020) 1174–1182.
[28] P. Xie, D. Wang, Y. Liu, J. Peng, Incorporating social vulnerability to assess population health risk due to heat stress in China, Acta Geograph. Sin. (2015) 1041–1051.

[29] Y. Wang, H. Wang, P. Cui, et al., Disaster effects of climate change and the associated scientific challenges, Chin. Sci. Bull. 69 (2024) 286–300, https://doi.org/10.1360/TB-2023-0325.
[30] J. Takakura, S. Fujimori, N. Hanasaki, T. Hasegawa, Y. Hirabayashi, Y. Honda, T. Iizumi, N. Kumano, C. Park, Z. Shen, others, Dependence of economic impacts of climate change on anthropogenically directed pathways, Nat. Clim. Change 9 (10) (2019) 737–741.
[31] W. Saeed, I. Haqiqi, Q. Kong, M. Huber, J.R. Buzan, S. Chonabayashi, K. Motohashi, T.W. Hertel, The poverty impacts of labor heat stress in west africa under a warming climate, Earth's Future 10 (11) (2022).
[32] J. Zong, L. Wang, C. Lu, Y. Du, Q. Wang, Mapping health vulnerability to short-term summer heat exposure based on a directional interaction network: hotspots and coping strategies, Sci. Total Environ. 881 (2023) 163401.
[33] F.N. Tonmoy, A. El-Zein, J. Hinkel, Assessment of vulnerability to climate change using indicators: a meta-analysis of the literature: assessment of vulnerability to climate change using indicators, WIREs Clim Change 5 (2014) 775–792.
[34] I. Keramitsoglou, et al., Urban thermal risk reduction: developing and implementing spatially explicit services for resilient cities, Sustain. Cities Soc. 34 (2017) 56–68.
[35] N. Krstic, W. Yuchi, H.C. Ho, B.B. Walker, A.J. Knudby, S.B. Henderson, The Heat Exposure Integrated Deprivation Index (HEIDI): a data-driven approach to quantifying neighborhood risk during extreme hot weather, Environ. Int. 109 (2017) 42–52, https://doi.org/10.1016/j.envint.2017.09.011.
[36] L. Anselin, Local indicators of spatial association—LISA, Geogr. Anal. 27 (1995) 93–115.
[37] L. Anselin, Chapter eight-the moran scatterplot as an ESDA tool to assess local instability in spatial association, Spatial Analytical 4 (1996) 121.
[38] C. Brunsdon, A.S. Fotheringham, M.E. Charlton, Geographically weighted regression: a method for exploring spatial nonstationarity, Geogr. Anal. 28 (4) (1996) 281–298.